Bi-Cu Electrolytes with Aminocarboxylate Chelators for Reversible Metal Electrodeposition at High pH for Dynamic Windows

Judy Y. Li, Madeline J. Leahy, Nikhil C. Bhoumik, Darren D. Miller, Desmond C. Madu, and Christopher J. Barile*

Department of Chemistry, University of Nevada, Reno, NV 89557

*E-mail: cbarile@unr.edu

Abstract

Dynamic windows, which possess electronically tunable light transmission, increase both the energy efficiency and aesthetics of spaces such as buildings and automobiles. Although reversible metal electrodeposition affords a promising approach to constructing high-performing dynamic windows, the acidic nature of the aqueous electrolytes frequently used in these windows has prevented their commercialization due to tin-doped indium oxide (ITO) etching. In this manuscript, we design neutral and alkaline electrolytes that support the reversible electrodeposition of Bi and Cu at rates comparable to existing acidic electrolytes. In these electrolytes, Bi3+ and Cu2+ are solubilized by using aminocarboxylate chelating ligands. By evaluating a series of ligands with varying denticities, we demonstrate that N-(2hydroxyethyl)ethylenedianmine-N,N',N'-triacetic acid (ED3A-OH) provides the optimal metal ion binding strength that enhances solubility while simultaneously supporting rapid metal electrodeposition. These results allow us to design alkaline ED3A-OH electrolytes that are compatible with ITO even after four weeks of immersion at 85°C. This manuscript thus demonstrates that chelating ligands can be utilized to design alkaline reversible metal electrodeposition electrolytes that support dynamic windows with robust shelf lives.

Introduction

Dynamic windows based on reversible metal electrodeposition are a promising technology for developing windows with electronically switchable transmission. Studies have shown that the incorporation of these windows into buildings results in an average of a 10% reduction in building energy consumption due to lighting, heating, and cooling savings. ^{1,2} In addition to buildings, dynamic windows could be used to improve the energy efficiency of automobiles, which is particularly important for electric vehicles in which battery capacity that goes towards air conditioning limits driving range. ³ Reversible metal electrodeposition can also be used for applications other than windows such as in displays and electronic paper. ^{4,5}

Over the last thirty years, several strategies have been explored to construct dynamic windows. The most studied strategy is to use electrochromic materials, which are materials that change optical properties upon application of a voltage.⁶ These electrochromic materials include transition metal oxides such as WO₃,^{7,8} polymers such as polythiophenes and polypyrroles,⁹⁻¹¹ and small molecules such as viologens.^{12,13} These materials can be prepared through a variety of different methods. For example, WO₃ is traditionally produced over the large areas needed for window deposition using sputter deposition,¹⁴ but solution-processed methods have also been developed.¹⁵

The use of metals as the optically active components of dynamic windows has several advantages over other strategies such as electrochromic materials. ¹⁶⁻¹⁸ First, metals are excellent at blocking light due to their high extinction coefficients. ¹⁹ As a result, only tens of nanometers of metals are needed to create opaque films as opposed to electrochromic materials, which typically require thicknesses of hundreds or thousands of nanometers to achieve comparable opacity levels. ²⁰⁻²⁴ Second, most metals are color neutral, which facilitates the construction of

devices with highly desirable clear-to-black transitions. Lastly, many metals are intrinsically durable materials that are stable towards light and heat.²⁵

In a dynamic window based on reversible metal electrodeposition, metal is electrodeposited onto a transparent working electrode such as tin-doped indium oxide (ITO) on glass to turn the device opaque, a reaction that is charge balanced by oxidation at a counter electrode, typically metal dissolution to soluble metal ions on a metal frame or transparent metal mesh. An opposite polarity is then applied to the device to induce metal dissolution on the working electrode to render the window clear. To gain information about the dynamics of reversible metal electrodeposition on the transparent electrode, three-electrode electrochemistry experiments can be performed using ITO on glass as the working electrode. Note that in these studies, the term "reversible" in reversible metal electrodeposition refers to the sequence of electrodepositing and dissolving metal from the working electrode and does not refer to the rate of electron transfer as does the term "reversible" in the classic electrochemical sense. 41

A wide range of metals has been explored for reversible electrodeposition in dynamic windows. ²⁶⁻³⁰ Previous research shows that Bi and Cu electrolytes facilitate fast, reversible, and color neutral metal electrodeposition over thousands of cycles. ³¹⁻³⁵ In aqueous electrolytes, most metal-based electrolytes that have been studied are acidic. These solutions tend to not be soluble under more alkaline conditions because of the formation of insoluble metal hydroxides. Indeed, standard Bi-Cu electrolytes form large quantities of insoluble Bi(OH)₃ at pH values greater than 2 as described by Equation 1. Indeed, the solubility product constant (K_{sp}) of Bi(OH)₃ is low at 3.2 x 10⁻⁴⁰ at 25°C. ³⁶

$$Bi^{3+}_{(aq)} + 3H_2O \rightleftharpoons Bi(OH)_{3(s)} + 3H^{+}_{(aq)}$$
 (1)

There are two main problems with acidic electrolytes in metal-based dynamic windows utilizing ITO. The first major issue is device shelf life. Acidic solutions slowly degrade the ITO.³⁷⁻³⁹ As ITO is immersed in the acidic electrolyte, the resistivity increases, and the working electrode will eventually become non-conductive, preventing device switching and reducing device lifetime. Because the average lifetime of a typical static window is 20 years, ⁴⁰ a dynamic window must cycle over 7,000 times during its service life if it is only switched between clear and dark states once a day. The second issue is that acidic solutions are more prone to deleterious H₂ gas evolution during cycling than neutral or alkaline solutions. According to the Nernst Equation, the thermodynamic potential for H₂ evolution is at -0.33 V vs. Ag/AgCl at pH 2, while it is -0.62 V vs. Ag/AgCl at pH 7.⁴¹ This negative shift in the voltage associated with the thermodynamics of H₂ evolution greatly increases the electrochemical stability window, allowing the voltage limit to be expanded during device operation. This shift in the thermodynamic voltage of H₂ evolution under alkaline conditions is important because H₂ evolution is kinetically facile on ITO electrodes.^{32,42}

To increase the pH of the solution, a method is needed to solubilize the Bi⁺³ ions. Chelating agents are ligands that bond metal ions, and thus they can be utilized to avoid metal values.⁴³ Previously, Bi^{3+} higher рН formation and solubilize at hydroxide ethylenediaminetetraacetic acid (EDTA) was used in Bi-Cu electrolytes to obtain an alkaline electrolyte.³⁷ However, while the shelf life of the dynamic window increased, device switching speeds were significantly reduced. EDTA is a hexadentate ligand that binds a metal ion through six different lone pairs. A high amount of denticity would presumably allow for more metal ion solubility, and an increase in metal ions would increase the switching speed. At the same time, however, a high denticity produces a more tightly bound complex and decreases the switching speed because the metal ion must disassociate from the metal-chelate complex before metal electrodeposition can occur. Therefore, we hypothesize that a balance must be struck between tight binding and the increased metal solubility it affords versus weak binding and the concomitant increase in metal electrodeposition kinetics.

Figure 1. Structures of EDTA (A), ED3A-OH (B), EDDA (C), and ED1A (D).

One way to produce a complex with a weaker binding constant is to lower the denticity of the ligand. Ligands analogous to EDTA include ethylenediaminetriacetic acid (ED3A), ethylenediaminediacetic acid (EDDA), and ethylenemonoamineacetic acid (ED1A). These variations of EDTA each have progressively one less acetic acid arm than the last, resulting in a progressive decrease in denticity (Figure 1). Another common ligand is N-(2-hydroxyethyl)ethylenedianmine-N,N',N'-triacetic acid (ED3A-OH), which is commercially available unlike ED3A. ED3A-OH possesses a denticity of five, but the molecule also contains a hydroxyl group that increases its solubility in aqueous solutions (Figure 1B).

In this manuscript, we investigate the use of these aminocarboxylate chelating ligands for designing soluble Bi-Cu electrolytes under neutral and alkaline conditions that facilitate reversible metal electrodeposition. Among the chelating ligands tested, ED3A-OH exhibits the best balance between Bi³⁺ solubility and reversible metal electrodeposition kinetics. We find that optimal aqueous Bi-Cu electrolytes containing ED3A-OH at high pH exhibit comparable electrodeposition kinetics to analogous Bi-Cu acidic electrolytes. Furthermore while acidic electrolytes etch ITO at room temperature, the alkaline Bi-Cu electrolytes with ED3A-OH designed here have the added benefit of not etching ITO even at 85°C.

Experimental

Chemicals were received from commercial sources and used without further purification. Ethylenediaminetetraacetic acid (99%), BiCl₃ (98%), CuCl₂ (99.9%), and LiClO₄ (99.9%) were purchased from Oakwood Chemicals. Ethylenediamine-*N*,*N*'-diacetic acid (98%), N-(2-hydroxyethyl)ethylenediaminetriacetic acid trisodium salt (99%), polyvinyl alcohol (98%, 61,000 molecular weight) and Cu(ClO₄)₂ (98%) were procured from Sigma-Aldrich. BiOClO₄ (96%) was purchased from Alfa Aesar. *N*-(2-aminoethyl)glycine (97%) was obtained from TCI America. All electrochemical studies were conducted using a VSP-300 Biologic potentiostat. Three-electrode experiments had their electrochemical potentials measured and reported with respect to a "no-leak" Ag/AgCl (3 M KCl) reference electrode (eDAQ) and used Pt wire as a counter electrode. All experiments were performed under air. Transmission spectra were measured with an Ocean Optics FLAME-S-VIS-NIR spectrometer using an Ocean Optics light source (HL2000-FHSA).

ITO on glass electrodes (Xin Yan, Inc., $10 \Omega \text{ sq}^{-1}$) were cleaned by sonicating in deionized H₂O with 5% Extran solution (Sigma-Aldrich) for 5 min, rinsing with water and

isopropanol, and sonicating in isopropanol for 5 min. The electrodes were subsequently dried under a stream of air. The cleaned ITO on glass electrodes were then modified with Pt nanoparticles. For Pt modification, the electrodes were first immersed in a 10 mM solution of 3-mercaptopropionic acid (Sigma-Aldrich, 99%) in ethanol (200 proof, Pharmco-Aaper) for at least 24 hours. Next, the electrodes were rinsed with ethanol and water before immersing them in dispersion of Pt nanoparticles in water (3 nm diameter, 250 ppm, Sigma-Aldrich) for an additional 24 hours. Finally, the electrodes were washed with water and heated for 20 min at 275°C. This protocol used for the self-assembly of Pt nanoparticles results in a density of 8,000 Pt nanoparticles per mm² as has been demonstrated through previous scanning electron microscopy (SEM) images. For all three-electrode experiments, the immersed geometric surface area of the working electrode was 1.5 cm², and electrochemical cells were assembled in a 2.0 cm by 2.0 cm glass cuvette. Electrolytes were pH adjusted using a concentrated aqueous solution of NaOH (Oakwood Chemicals, 99%). SEM images were recorded using a JEOL JSM-6010LA microscope using an accelerating voltage of 10 kV.

Results and Discussion

Commonly employed Bi-Cu electrolytes consist of Bi and Cu halides that are adjusted to pH ~ 2 to maintain metal ion solubility. ^{21,32,33,44} We therefore first evaluated a series of aminocarboxylate chelating agents for use in Bi-Cu electrolytes consisting of 20 mM BiCl₃ and 20 mM CuCl₂ at pH 7. At neutral pH, the Bi-Cu electrolyte could not be solubilized with ED1A. With a denticity of only three, the binding constant of ED1A to Bi³⁺ and Cu²⁺ is evidently too weak to prevent the formation of insoluble Bi(OH)₃ and Cu(OH)₂. However, when utilizing EDDA, ED3A-OH, or EDTA, all of which have higher denticities, the electrolytes are completely soluble with 0.2 M of the chelating agent.

Figure 2A presents cyclic voltammograms (CVs) of reversible metal electrodeposition on Pt-modified ITO working electrodes. A sparse distribution of Pt nanoparticles is used as an inert seed layer on the ITO electrodes because this layer increases the uniformity and reversibility of metal electrodeposition as has been shown previously for a wide range of reversible metal electrodeposition systems. The second cycles of all CVs in this manuscript are presented rather than first because the second cycle is a more accurate representation of the overall electrochemical behavior of each system. During the first CV cycle, metal seeds are deposited in grain boundaries and other defect sites on the ITO working electrode. Metal electrodeposition during the second and subsequent cycles occurs on these metal seeds that are established during the first cycle such that the CVs of the second and later cycles are typically consistent with one another (Figure S1).

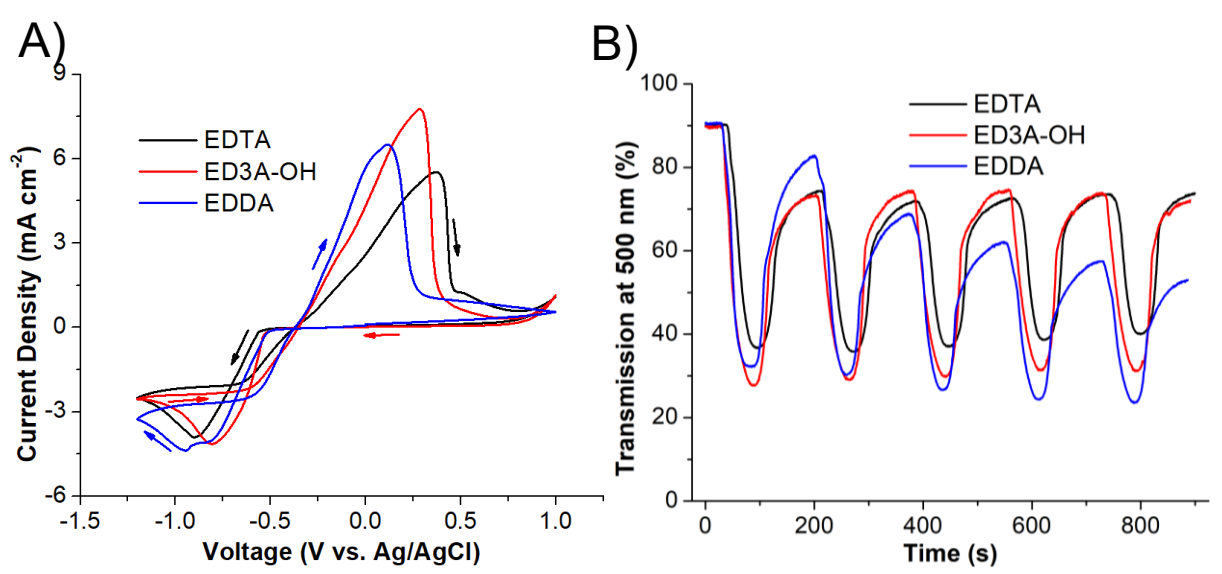


Figure 2. Cyclic voltammetry at a scan rate of 25 mV s⁻¹ (A) and corresponding transmission at 500 nm (B) of an ITO on glass working electrode in electrolytes containing 20 mM BiCl₃, 20 mM CuCl₂ and 0.2 M of EDTA (black line), ED3A-OH (red line), or EDDA (blue line) at pH 7.

The general shape of the CVs with EDDA, EDA3-OH, and EDTA are similar. Cathodic current associated with Bi and Cu electrodeposition on the ITO begins at potentials more negative than -0.5 V. A diffusion-limited peak associated with this metal electrodeposition

appears at more negative potentials. On the return scan, an anodic peak due to dissolution (stripping) of metal on the working electrode is evident. The onset potentials of metal electrodeposition for the three electrolytes become increasingly more negative in the order of EDTA > ED3A-OH ~ EDDA. This trend follows the denticity order of the three ligands with EDTA, the highest denticity ligand, resulting in the most negative deposition onset potential. The metal EDTA complexes, which have the highest stability constants, expectedly result in a larger thermodynamic penalty for dissociation and subsequent metal electrodeposition.

Figure 2B presents the transmission of the ITO working electrode during the first five CV cycles of reversible metal electrodeposition in each of the three electrolytes. Corresponding transmission versus voltage curves are displayed in Figure S2. The electrode transmission in all three electrolytes does not return to its original value of ~90% after the first CV cycle due in part to the establishment of metal nuclei as described earlier. During the subsequent four cycles, however, the transmission is reversible with the EDTA electrolyte (Figure 2B, black line). This decrease in maximum electrode transmission results in a corresponding decrease in minimum transmission during cycling. In contrast, the maximum electrode transmission in the EDDA electrolyte consistently declines with each subsequent cycle (Figure 2B, blue line). In other words, the EDTA electrolyte supports mostly optically reversible Bi and Cu electrodeposition, while the EDDA electrolyte does not. Presumably, the greater favorability to form metal EDTA complexes as compared to metal EDDA complexes increases metal stripping kinetics, thus improving the optical reversibility of the EDTA electrolyte. Like the EDTA electrolyte, the ED3A-OH also facilitates mostly optically reversible metal electrodeposition after the first CV cycle (Figure 2B, red line). However, the minimum transmission of the working electrode in the ED3A-OH electrolyte during each cycle is ~30%, while the same value is only ~40% in the

EDTA electrolyte. The lower attained transmission in the ED3A-OH systems suggests that this electrolyte supports faster metal electrodeposition than EDTA. Indeed, the magnitude of the diffusion-limited current density in the ED3A-OH CV is greater than that of EDTA (compare red line to black line in Figure 2A). This result is rationalized by the weaker binding constant of ED3A-OH to Bi³⁺ and Cu²⁺ due its lower denticity, which accelerates metal deposition kinetics. Given the advantageous optoelectronic properties of the ED3A-OH electrolyte both in terms of its optical reversibility and its faster electrodeposition kinetics, we elected to systematically study and develop ED3A-OH electrolytes in the remainder of this manuscript.

Recently, a pH 2 Bi-Cu electrolyte using perchlorates was designed that displays enhanced cycleability and a wide voltage stability window that facilitates device scale up. 48 We wondered if the strategy of using ED3A-OH could be extended to perchlorate electrolytes to increase their pH. Although the solubility of metal ions in perchlorate electrolytes is less than that of chloride electrolytes, perchlorate electrolytes are advantageous for studying the effect of the chelating ligand because perchlorate is a non-coordinating anion. Figure 3 shows CVs and corresponding transmission profiles of the ITO working electrodes in electrolytes containing BiOClO₄, Cu(ClO₄)₂, and 100 mM ED3A-OH at pH values of 2 and 7. Both the onset potential and the diffusion-limited peak for metal electrodeposition are about 0.16 V more negative in the pH 7 electrolyte as compared to pH 2. The reported pK_a values for the two amines of ED3A-OH are 9.9 and 5.4, the pK_a of the first carboxylic acid is 2.4, and the remaining two carboxylic acids have pK_a values less than 2.⁴⁹ As a result, at pH 2, the two amine groups of ED3A-OH are protonated, two of the carboxylates are deprotonated, and the third carboxylate is mostly protonated. In contrast, at pH 7, all three carboxylates and one of the amines are fully deprotonated. Thus at pH 7, the more negatively charged state of ED3A-OH increases its binding

strength to the positively charged Bi³⁺ and Cu²⁺ ions. In other words, the ability of ED3A-OH to complex metal cations at pH 7 much more strongly than at pH 2 is the key difference between these two electrolytes. For this reason, it is more difficult to dissociate the Bi and Cu ED3A-OH complexes during metal electrodeposition at pH 7, which results in a negative shift in the onset potential for metal electrodeposition. Nonetheless, the transmission values of the working electrode during CV cycles of the perchlorate electrolytes at pH 2 and pH 7 are both reversible (Figure 3B). Interestingly, for the pH 7 case (Figure 3B, red line), the transmission curve consistently possesses a sharp, low-magnitude decrease in transmission at the onset of metal stripping. Although the exact origin of this phenomenon is unclear, we hypothesize it is due to the transient formation of insoluble species at the electrode interface such as metal hydroxides that decrease electrode transmission before chelation subsequently occurs to form soluble complexes.

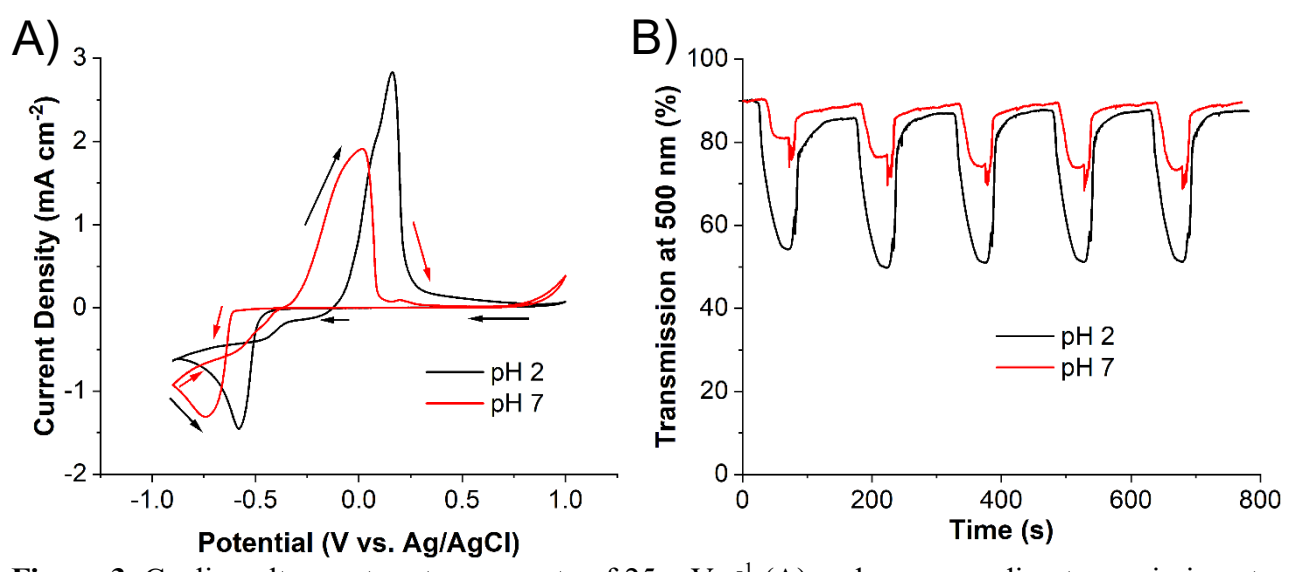


Figure 3. Cyclic voltammetry at a scan rate of 25 mV s⁻¹ (A) and corresponding transmission at 500 nm (B) of an ITO on glass working electrode in an electrolyte containing 5 mM Cu(ClO₄)₂, 5 mM BiOClO₄, 10 mM HClO₄, 1 M LiClO₄, and 100 mM ED3A-OH at pH 2 (black line) and 7 (red line).

To further interrogate the nature of ED3A-OH binding in the Bi-Cu perchlorate electrolyte, we performed spectroelectrochemical measurements using electrolytes with varying ED3A-OH concentrations. With 5 mM or 10 mM ED3A-OH, the Bi and Cu salts are not fully soluble at pH 7, so electrolytes at pH 2 were instead studied. Unlike the CVs discussed thus far in this manuscript, the CV of the electrolyte with 5 mM ED3A-OH displays two reductive peaks (Figure 4A, black line). The peak at around -0.5 V is ascribed to Bi electrodeposition from Bi complexes of ED3A-OH, while the peak at around -0.3 V is assigned to Cu electrodeposition from Cu(H₂O)₆²⁺. Peak assignments are made from corresponding voltammetry with only Bi³⁺ and only Cu²⁺ in the electrolytes (Figure S3). With only 5 mM ED3A-OH compared to 5 mM each of BiOClO₄ and Cu(ClO₄)₂, there is only enough ED3A-OH present to bind the Bi³⁺. The binding constant of ED3A-OH is much stronger to Bi³⁺ than to Cu²⁺ because of the greater charger of Bi³⁺. The relative binding constants of EDTA to these two metal ions provide an illustrative analogy with EDTA binding approximately one billion times more tightly to Bi3+ than Cu²⁺.50 Because Cu²⁺ is not bound to ED3A-OH in the 5 mM ED3A-OH electrolyte, Cu electrodeposits at a significantly more positive potential than Bi electrodeposition from its ED3A-OH complex. Increasing the ED3A-OH concentration to 10 mM similarly gives rise to two reductive peaks in the CV, but the current density associated with the Cu deposition peak from Cu(H₂O)₆²⁺ is much reduced because at this higher concentration of ED3A-OH, most of the Cu²⁺ is chelated (Figure 4A, red line).

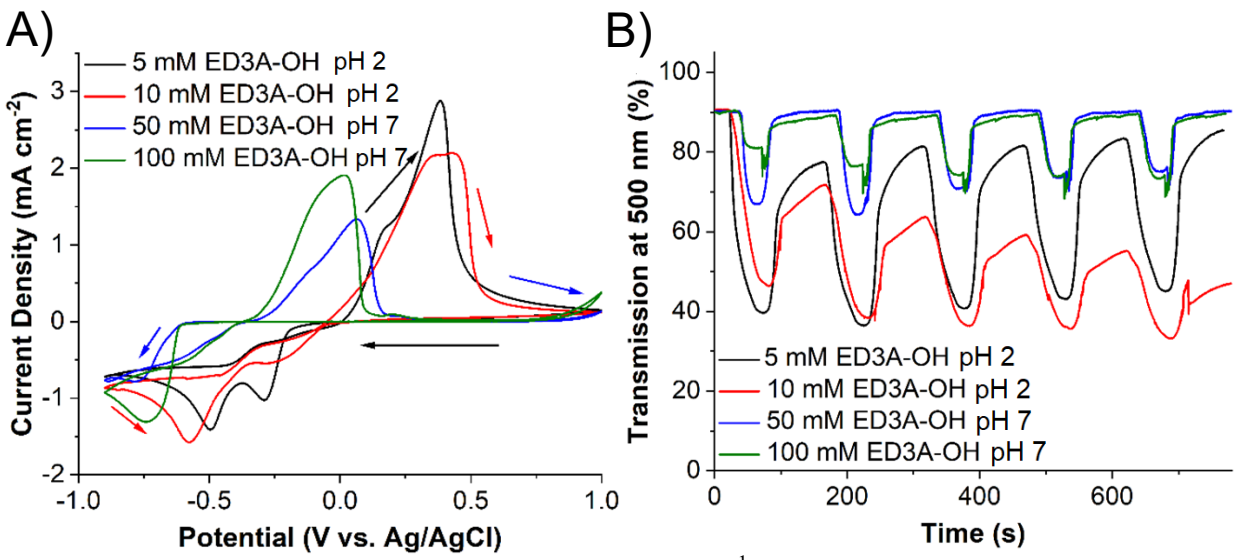


Figure 4. Cyclic voltammetry at a scan rate of 25 mV s⁻¹ (A) and corresponding transmission at 500 nm (B) of an ITO on glass working electrode in an electrolyte containing 5 mM Cu(ClO₄)₂, 5 mM BiOClO₄, 10 mM HClO₄, 1 M LiClO₄, and various concentrations of ED3A-OH: 5 mM (black line) at pH 2, 10 mM (red line) at pH 2, 50 mM (blue line) at pH 7, and 100 mM (green line) at pH 7.

At the higher concentrations of 50 mM and 100 mM ED3A-OH, the Bi-Cu perchlorate electrolytes are soluble at pH 7 (Figure 4, green and blue lines). Both of these electrolytes possess negatively-shifted deposition onset and peak potentials compared to the pH 2 electrolytes due to the proton-coupled nature of electrodeposition as mentioned in the discussion of Figure 3. Although the origin of the differences in the current density of the 50 mM and 100 mM ED3A-OH is unclear, the 100 mM ED3A-OH electrolyte exhibits optically reversible transmission and more consistent minimum and maximum transmission values during each CV cycle as compared to the 50 mM ED3A-OH electrolyte. For this reason, we use 100 mM ED3A-OH in all subsequent studies aimed at further improving the spectroelectrochemical attributes of pH 7 Bi-Cu perchlorate electrolytes.

For the optically reversible pH 7 systems, there are slight differences in the transmission profile during each cycle. SEM images of the electrodeposits formed by halting the CV at -0.9 V demonstrate that the nucleation density of the electrodeposits is greater during cycle 2 than cycle

1 for the pH 7 100 mM ED3A-OH electrolyte (Figure S4). This finding explains why the minimum attained electrode transmission for this electrode is less during cycle 2 than cycle 1 (Figure 4, green line).

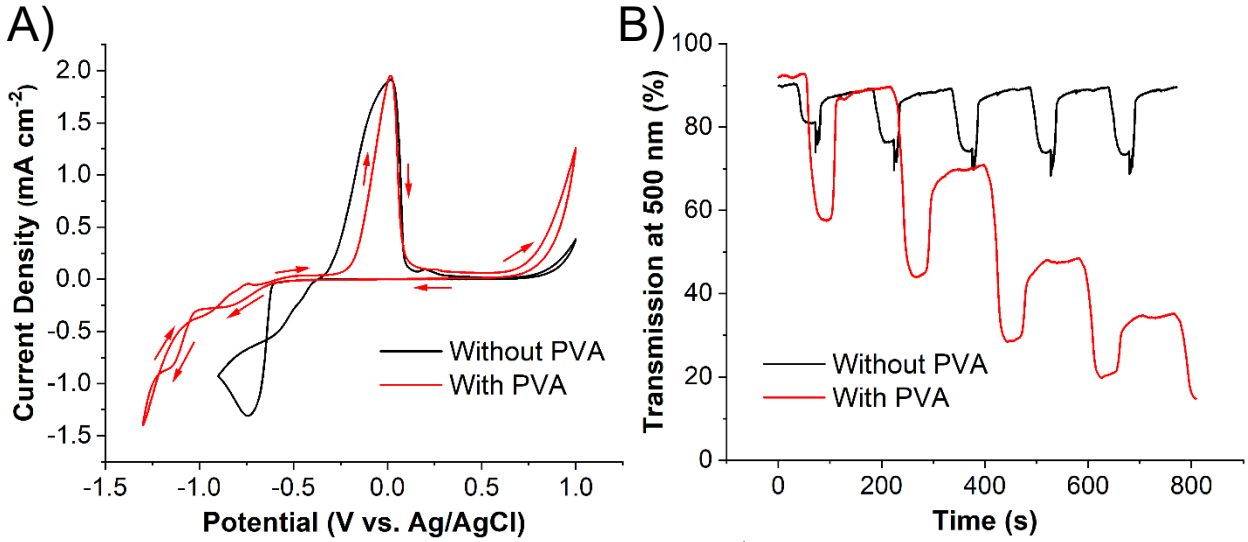


Figure 5. Cyclic voltammetry at a scan rate of 25 mV s⁻¹ (A) and corresponding transmission at 500 nm (B) of an ITO on glass working electrode in electrolytes containing 5 mM Cu(ClO₄)₂, 5 mM BiOClO₄, 10 mM HClO₄, 1 M LiClO₄, 100 mM ED3A-OH at pH 7 without (black line) and with (red line) 1 wt. % PVA.

In an attempt to increase the optical contrast of the Bi-Cu perchlorate pH 7 electrolyte, 1 wt. % of polyvinyl alcohol (PVA) was added to the electrolyte (Figures 5 and S5). PVA is a polymer that suppresses dendritic electrodeposit growth and promotes a compact morphology through an adsorption mechanism. The adsorbed polymer layer distributes the charge over a uniform layer allowing the positive ions to interact within a flatter layer. Without the polymer, the metal electrodeposits form dendritic sites because of localized electric fields. The optical contrast, defined as the maximum and minimum transmission value of the working electrode during each CV cycle, is greater than 30% for the electrolyte with PVA (Figure 5B, red line), while it is only about 15% for the same electrolyte without PVA (Figure 5B, black line). Unfortunately, the electrode transmission is not optically reversible during cycling, and the maximum attained transmission decreases with each subsequent cycle. The addition of PVA

results in significant anodic current density in the CV at voltages more positive than 0.7 V (Figure 5A, red line). This current is due to the O₂ evolution reaction (OER), which at pH 7 possesses a standard reduction potential of 0.61 V vs. Ag/AgCl.⁵² With the generation of O₂ at the electrode surface, residual metal on the working electrode resulting from incomplete stripping has a greater propensity to convert to metal oxides, which cannot be electrochemically dissolved during subsequent cycling. The formation of metal oxides facilitated by the OER thus explains the poor optical reversibility of this PVA electrolyte.

In reversible metal electrodeposition electrolytes, the addition of more metal ions is a straightforward method of increasing electrodeposition kinetics. We thus evaluated the spectroelectrochemical properties of Bi-Cu electrolytes with PVA with increasing concentrations of metal ions (Figure 6). With 100 mM ED3A-OH, we determined that the maximum solubility of BiOClO4 is 18.5 mM at pH 7. We then investigated the effect of different concentrations of Cu(ClO4)2 at the 18.5 mM solubility limit of BiOClO4. The transmission data show that all three of the electrolytes tested exhibit fairly reversible optics (Figure 6B). With increasing Cu(ClO4)2 concentrations, the contrast ratio during the CV increases, reaching a value of greater than 75% for the electrolyte with 18.5 mM Cu(ClO4)2. The transmission profile across all visible light wavelengths for this electrolyte is displayed in Figure S6. This contrast ratio represents light modulation capabilities and kinetics that are comparable to previously developed Bi-Cu perchlorate electrolytes at pH 2.⁴⁸

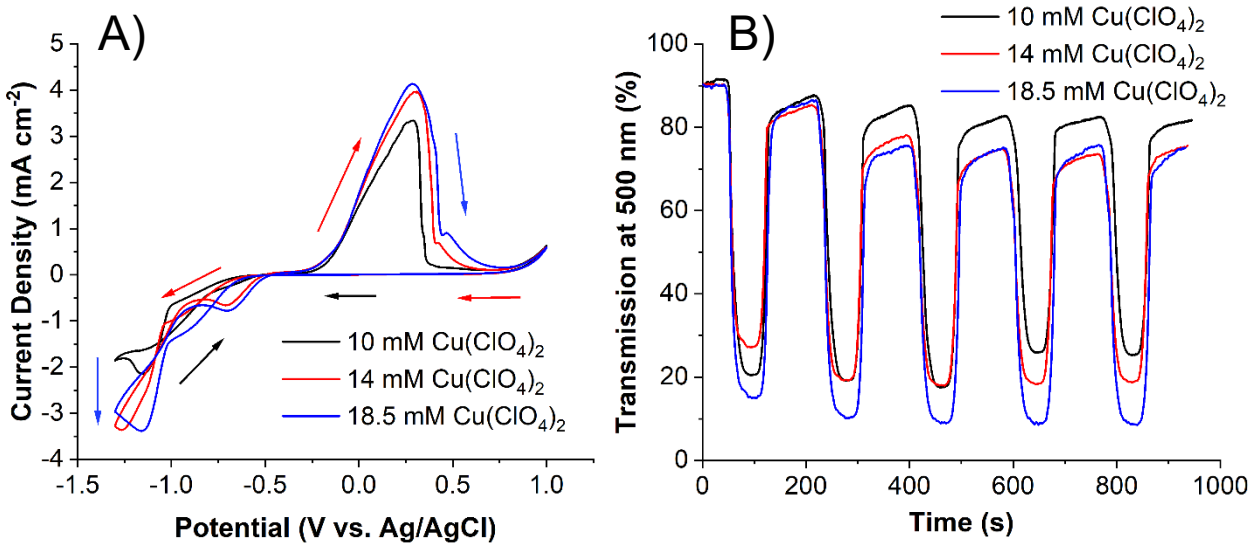


Figure 6. Cyclic voltammetry at a scan rate of 25 mV s⁻¹ (A) and corresponding transmission at 500 nm (B) of a Pt-ITO on glass working electrode in an electrolyte containing 18.5 mM BiOClO₄, 10 mM HClO₄, 1 M LiClO₄, 100 mM ED3A-OH, 1 wt. % PVA and various concentrations of Cu(ClO₄)₂: 10 mM (black line) at pH 7, 14 mM (red line) at pH 7, and 18.5 mM (blue line) at pH 7.

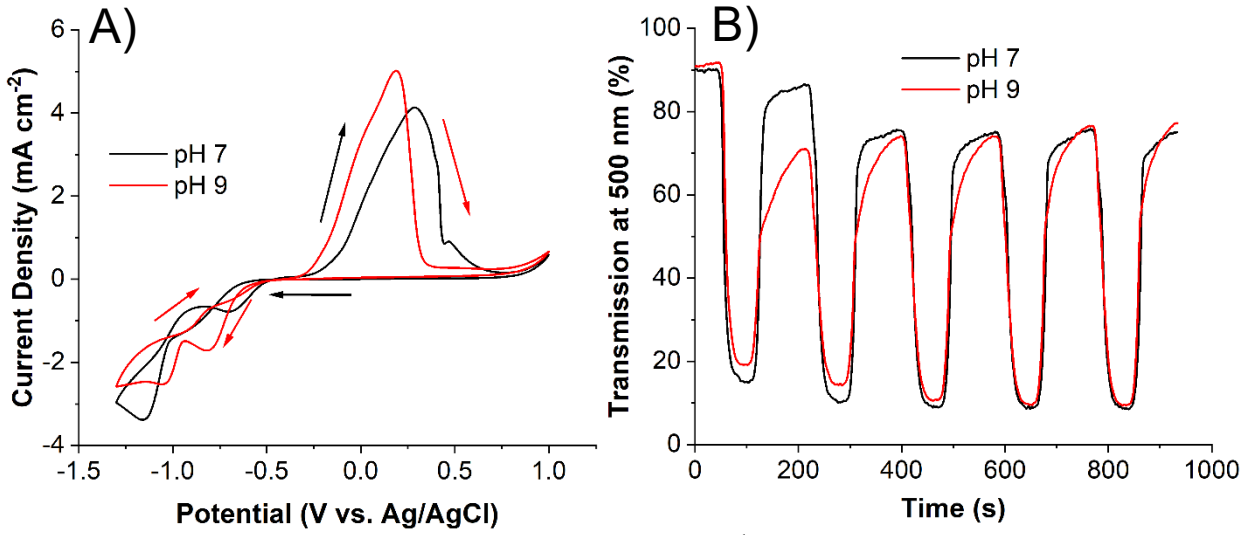


Figure 7. Cyclic voltammetry at a scan rate of 25 mV s⁻¹ (A) and corresponding transmission at 500 nm (B) of a Pt-ITO on glass working electrode in an electrolyte containing 18.5 mM Cu(ClO₄)₂, 18.5 mM BiOClO₄, 10 mM HClO₄, 1 M LiClO₄, 100 mM ED3A-OH, and 1 wt. % PVA at pH 7 (black line) and pH 9 (red line).

We also evaluated the electrolyte with 18.5 mM BiOClO₄ and 18.5 mM Cu(ClO₄)₂ at pH 9, which also exhibits a transmission profile that is mostly optically reversible (Figure 7). These experiments demonstrate that alkaline Bi-Cu electrolytes can be designed that support reversible

metal electrodeposition with high optical contrast. The most relevant kinetic attribute of reversible metal electrodeposition electrolytes for dynamic windows is their optical switching speed. To quantitatively compare the metal electrodeposition kinetics among the pH 2, pH 7, and pH 9 electrolytes, we measured the transmission at 500 nm of ITO electrodes while performing chronoamperometry at -1.4 V vs. Ag/AgCl (Figure S7). Starting from an initial transmission of 90%, the electrodes reach 1% transmission after 31 s, 49 s, and 57 s for the pH 2, pH 7, and pH 9 electrolytes, respectively. These data indicate that progressively more alkaline electrolytes switch more slowly. Despite the reduced switching speeds, the enhanced stabilities of the more basic electrolytes towards ITO makes them important for dynamic window applications (*vide infra*).

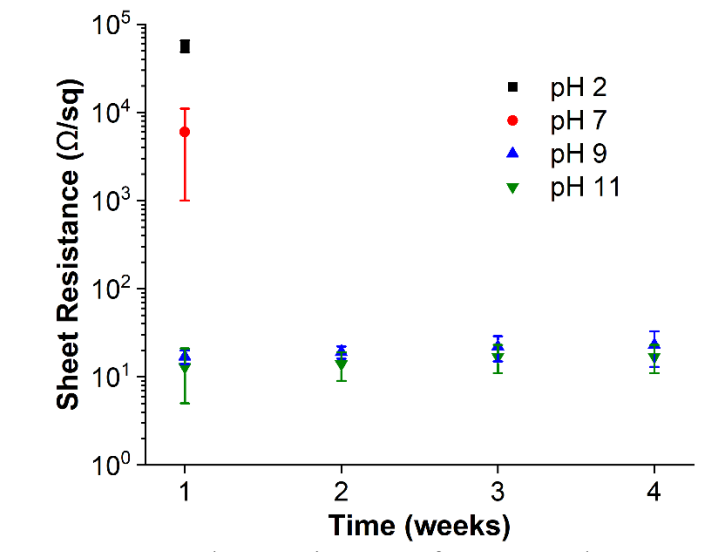


Figure 8. Sheet resistance of Pt-ITO substrates after immersion at 85°C in a pH 2 electrolyte containing 5 mM Cu(ClO₄)₂, 5 mM BiOClO₄, 10 mM HClO₄, and 1 M LiClO₄ (black point) and 18.5 mM Cu(ClO₄)₂, 18.5 mM BiOClO₄, 10 mM HClO₄, 1 M LiClO₄, 100 mM ED3A-OH, and 1 wt. % PVA at pH 7 (red point), pH 9 (blue points), and pH 11 (green points).

As discussed in the Introduction, a key disadvantage of acidic electrolytes is that they slowly etch ITO at room temperature, which gives dynamic windows that utilize acidic electrolytes poor shelf lives.³⁷ The sheet resistance of the ITO working electrode can be measured after immersion in an electrolyte as a proxy for assessing device shelf life. Moreover, immersion of the ITO in an electrolyte at 85°C is an accelerated aging test.⁵³ After one week of

immersion in Bi-Cu ED3A-OH electrolytes at pH 2 or pH 7 at 85°C, the ITO sheet resistance increases dramatically to > 1,000 Ω /sq from its original value of 15 Ω /sq. This large increase in sheet resistance prevents further switching of the electrodes, and after two weeks of immersion, the ITO electrode becomes completely nonconductive. In contrast, the sheet resistances of ITO electrodes immersed in the Bi-Cu ED3A-OH electrolytes at pH 9 or pH 11 at 85°C do not significantly increase even after four weeks. These findings indicate that alkaline Bi-Cu ED3A-OH electrolytes can support the construction of dynamic windows with robust shelf lives.

Conclusions

A series of aminocarboxylate chelating ligands were evaluated for their ability to increase the solubility of Bi and Cu ions at high pH to enable the design of neutral and alkaline Bi-Cu electrolytes that support reversible metal electrodeposition on ITO transparent conducting electrodes, which are commonly used in dynamic windows. We determined that ED3A-OH with a denticity of five affords the optimal balance between tight metal ion binding, which enhances solubility, and loose metal ion binding, which facilitates reversible metal electrodeposition. We subsequently demonstrate that neutral and alkaline Bi-Cu electrolytes with ED3A-OH facilitate optically reversible metal electrodeposition with optical contrasts that are comparable with standard acidic Bi-Cu electrolytes. Importantly, these new alkaline Bi-Cu electrolytes do not etch ITO even after immersion for four weeks at 85°C, indicating that these electrolytes allow for the design of dynamic windows with excellent shelf lives.

Acknowledgment

This material is based upon work supported by the National Science Foundation Award under Grant No. ECCS2127308. We also acknowledge the Shared Instrumentation Laboratory in the Department of Chemistry at the University of Nevada, Reno (UNR). SEM-EDX analysis was

performed in the Mackay Microbeam Laboratory at UNR, and we thank J. DesOrmeau for the

kind assistance.

References

- 1. E. Lee, E., M. Yazdanian and S. Selkowitz. *The Energy-Savings Potential of Electrochromic Windows in the US Commercial Buildings Sector*, Lawrence Berkeley National Laboratory, LBNL-54966 (2004).
- 2. Energy Savings Guide, View Glass, Inc. http://viewglass.com/assets/pdfs/workplace-white-paper.pdf, accessed 5/3/2023
- 3. M. A. Jeffers, L. Chaney and J. P. Rugh, SAE International, 01-0355, 1 (2015).
- 4. J. P. Ziegler and B. M. Howard, Sol. Energ. Mater. Sol. C, 39, 317 (1995).
- 5. S. Hirata, T. Tsuji, Y. Kato and C. Adachi, Adv. Funct. Mater., 22, 4195 (2012).
- 6. R. J. Mortimer, Chem. Soc. Rev., 26, 147 (1997).
- 7. W. Wu, M. Wang, J. Ma, Y. Cao and Y. Deng, Adv. Electron. Mater., 4, 1800185 (2018).
- 8. D. T. Gillaspie, R. C. Tenent and A. C. Dillon, J. Mater. Chem., 20, 9585 (2010).
- 9. A. Chaudhary, D. K. Pathak, M. Tanwar, P. Yogi, P. R. Sagdeo and R. Kumar, *ACS Appl. Electron. Mater.*, **1**, 58 (2019).
- 10. G. A. Sotzing, J. R. Reynolds and P. J. Steel, Chem. Mater., 8, 882 (1996).
- 11. P. Camurku, RSC Adv., 4, 55832 (2014).
- 12. K. W. Shah, S. Wang, D. X. Y. Soo and J. Xu, *Polymers*, 11, 1839 (2019).
- 13. J. Palenzuela, A. Vinuales, I. Odriozola, G. Cabanero, H. J. Grande and V. Ruiz, *ACS Appl. Mater. Inter.*, **6**, 14562 (2014).
- 14. G. Atak, I. B. Pehlivan, J. Montero, C. G. Granqvist and G. A. Niklasson, *Electrochim. Acta*, **20**, 137233 (2021).
- 15. M. Yang, J. Wang, S. Zhang, L. Wang, Z. Zhang, Y. Wang, C. Niu and Y. Lv, *Solid State Sci.*, **132**, 106990 (2022).
- 16. V. K. Thakur, G. Ding, J. Ma, P. S. Lee and X. Lu, Adv. Mater., 24, 4071 (2012).
- 17. P. Shi, C. M. Amb, E. P. Knott, E. J. Thompson, D. Y. Liu, J. Mei, A. L. Dyer and J. R. Reynolds, *Adv. Mater.*, **22**, 4949 (2010).
- 18. G. A. Niklasson and C. G. Granqvist, J. Mat. Chem., 17, 127 (2007).
- 19. O. S. Heavens, *Optical Properties of Thin Solid Films*, Dover Publications, Inc., New York (1965).
- 20. S. M. Islam and C. J. Barile, ACS Appl. Mater. Inter., 11, 40043 (2019).
- 21. S. M. Islam, C. N. Fini and C. J. Barile, J. Electrochem. Soc., 166, D333 (2019).
- 22. L. R. Savagian, A. M. Österholm, D. E. Shen, D. T. Christiansen, M. Kuepfert and J. R. Reynolds, *Adv. Opt. Mater.*, **6**, 1800594 (2018).
- 23. C. J. Barile, D. J. Slotcavage and M. D. McGehee, Chem. Mater., 28, 1439 (2016).
- 24. T. Abidin, Q. Zhang, K. L. Wang and D. J. Liaw, Polymer, 55, 5293 (2014).
- 25. N. N. Greenwood and A. Earnshaw, *Chemistry of the Elements*, Butterworth-Heinemann, Oxford, U. K. (1997).
- 26. X. Guo, J. Chen, A. L. S. Eh, W. C. Poh, F. Jiang, F. Jiang, J. Chen and P. S. Lee, *ACS Appl. Mater. Inter.*, **14**, 20237 (2022).
- 27. D. C. Madu, M. V. Lilo, A. A. Thompson, H. Pan, M. D. McGehee and C. J. Barile, *ACS Appl. Mater. Inter.*, **14**, 47810 (2022).

- 28. L. S. Arvisu, A. A. Palma, S. M. Islam and C. J. Barile, *J. Electrochem. Soc.*, **169**, 072502 (2022).
- 29. S. Kimura, K. Nakamura and N. Kobayashi, Sol. Energ. Mater. Sol. C., 205, 110247 (2020).
- 30. C. Park, S. Seo, H. Shin, B. D. Sarwade, J. Na and E. Kim, Chem. Sci., 6, 596 (2015).
- 31. G. K. A. Alcaraz, J. S. Juarez-Rolon, N. A. Burpee and C. J. Barile, *J. Mat. Chem. C*, **6**, 2132 (2018).
- 32. T. S. Hernandez, C. J. Barile, M. T. Strand, T. E. Dayrit, D. J. Slotcavage and M. D. McGehee, *ACS Energy Lett.*, **3**, 104 (2018).
- 33. S. M. Islam, T. S. Hernandez, M. D. McGehee and C. J. Barile, *Nat. Energ.*, 4, 223 (2019).
- 34. B. M. Howard and J. P. Ziegler, Sol. Energ. Mater. Sol. C., 39, 309 (1995).
- 35. J. P. Ziegler and B. M. Howard, Sol. Energ. Mater. Sol. C., 39, 317 (1995).
- 36. T. L. Brown, H. E. LeMay, B. E. Bursten, C. J. Murphy, P. M. Woodward and M. W. Stoltzfus, *Chemistry: The Central Science*, 14th ed., Pearson Education, London (2017)
- 37. D. D. Miller, J. Y. Li, S. M. Islam, J. F. Jeanetta and C. J. Barile, *J. Mat. Chem. C*, **8**, 1826 (2020).
- 38. J. E. A. M. van den Meerakker, P. C. Baarslag and M. Scholten, *J. Electrochem. Soc.*, **142**, 2321 (1995).
- 39. T. H. Tsai and Y. F. Wu, Microelectron. Eng. 83, 536 (2006).
- 40. J. Salazar, *Electronic Theses and Dissertations*, "Life Cycle Assessment Case Study of North American Residential Windows," University of British Columbia (2007).
- 41. A. J. Bard and L. R. Faulkner, *Electrochemical Methods: Fundamentals and Applications*, John Wiley & Sons, Inc., Hoboken, NJ (2001).
- 42. J. D. Benck, B. A. Pinaud, Y. Gorlin and T. F. Jaramillo, *PLoS One*, **9**, e107942 (2014).
- 43. S. Franchi, V. Di Marco and M. Tosato, Nucl. Med. Biol., 114-115, 168 (2022).
- 44. C. L. DeFoor, J. F. Jeanetta and C. J. Barile, ACS Appl. Electron. Mater., 2, 290 (2020).
- 45. M. T. Strand, C. J. Barile, T. S. Hernandez, T. E. Dayrit, L. Bertoluzzi, D. J. Slotcavage and M. D. McGehee, *ACS Energy Lett.*, **3**, 2823 (2018).
- 46. C. J. Barile, D. J. Slotcavage, J. Hou, M. T. Strand, T. S. Hernandez and M. D. McGehee, *Joule*, 1, 133 (2017).
- 47. D. C. Madu, S. M. Islam, H. Pan and C. J. Barile, J. Mat. Chem. C, 9, 6297 (2021).
- 48. T. S. Hernandez, M. Alshurafa, M. T. Strand, A. L. Yeang, M. G. Danner, C. J. Barile and M. D. McGehee, *Joule*, 4, 1501 (2020).
- 49. M. P. Singh, Orient. J. Chem., 20, 407 (2004).
- 50. D. A. Skoog, D. M. West, F. J. Holler and S. R. Crouch, *Fundamentals of Analytical Chemistry*, Brooks/Cole (2004).
- 51. M. T. Strand, T. S. Hernandez, M. G. Danner, A. L. Yeang, N. Jarvey, C. J. Barile and M. D. McGehee, *Nat. Energ.*, **6**, 546 (2021).
- 52. M. Tahir, L. Pan, F. Idrees, X. Zhang, L. Wang, J.-J. Zou and Z. L. Wang, *Nano Energ.*, **37**, 136 (2017).
- 53. American Society for Testing and Materials, ASTM E2141-14, Standard Test Method for Accelerated Aging of Electrochromic Devices in Sealed Insulating Glass Units.